Hindawi
IET Signal Processing
Volume 2024, Article ID 6664937, 8 pages
https://doi.org/10.1049/2024/6664937

Research Article

Critical Design Considerations on Continuous Frequency Modulation Localization Systems

Belal Al-Qudsi[1], **Mohammed El-Shennawy**[1], **Niko Joram**[1], **Marco Gunia**[1] and **Frank Ellinger**[1,2]

[1]*Chair for Circuit Design and Network Theory, Technische Universität Dresden, Dresden, Germany*
[2]*Centre for Tactile Internet with Human-in-the-Loop (CeTI), Dresden, Germany*

Correspondence should be addressed to Belal Al-Qudsi; belal.alqudsi@tu-dresden.de

Received 21 July 2023; Revised 20 November 2023; Accepted 22 February 2024; Published 4 April 2024

Academic Editor: Richard Dansereau

Real-time locating systems (RTLSs) suffer from clock synchronization inaccuracy among their distributed reference nodes. Conventional systems require periodic time synchronization and typically necessitate a two-way ranging (TWR) clock synchronization protocol to eliminate their measurement errors. Particularly, frequency-modulated continuous-wave (FMCW) time-based location systems pose unique design considerations on the TWR that have a significant impact on the quality of their measurements. In this paper, a valid operation design diagram is proposed for the case of an FMCW time-based TWR synchronization protocol. The proposed diagram represents an intersection area of two boundary curves that indicate the functionality of the system at a given frequency bandwidth, spectral length, and clock synchronization ambiguity. It presents an intuitive illustration of the measurement's expected accuracy by indicating a larger intersection area for relaxed design conditions and vice versa. Furthermore, the absence of a working condition can easily be detected before proceeding with the actual system development. To demonstrate the feasibility of the proposed diagram, four scenarios with different design constraints were evaluated in a Monte-Carlo model of a basic TWR system. Moreover, an experimental measurement setup demonstrated the validity of the proposed diagram. Both the simulation and experimental outcomes show that the indicated valid conditions and the distribution of the measurements' accuracy are in very good agreement.

1. Introduction

Classical frequency-modulated continuous-wave (FMCW) radar-based systems measure the distance to passive objects by transmitting a frequency-modulated signal and processing its received reflections in a typical signal-mixing operation [1]. In contrast, a conventional application of the FMCW technique is distance measurements between active transceiver nodes, also known as secondary radar-based systems, which conduct core measures of other emergent complex systems such as accurate real-time locating systems (RTLSs) [2, 3]. Particularly, two transceiver nodes interact with each other; thus, the system no longer measures the distance to a passive object but between two transceiver nodes. Such a time measurement essentially requires carrying out a two-way ranging (TWR) time synchronization protocol to eliminate the measurement inaccuracy caused by the distributed clock timing issue [4]. In general, engineering an FMCW-based system involves several well-defined design criteria, such as signal duration, bandwidth, sampling rate, and chirp modulation rate [1, 5]. Many of the system components of the classical FMCW system, as well as its signal processing techniques, are indeed applied also in the active ranging system. Nevertheless, additional design considerations are crucial for carrying out the TWR. One challenge that distinguishes it from the passive system is the lack of time synchronization between its processed chirp signals. Thus, coarse time synchronization, which is typically realized by an auxiliary system, is essential to trigger the distributed nodes and bring them to an operational synchronization condition. In fact, the design of such a system poses challenging tradeoffs among its signal bandwidth, signal processing complexity, update rate, and the synchronization time ambiguity that are not only challenging to balance but also critical for the core operation of the localization system.

In this paper, a valid operation design diagram for the TWR FMCW-based system is proposed. It indicates the

validity of the essential design conditions at a given frequency bandwidth, spectral length, and maximum time ambiguity. In order to demonstrate the feasibility of the proposed diagram, four design scenarios with different design constraints were evaluated in a Monte-Carlo model of an FMCW TWR system. Thereafter, an experimental setup was carried out for evaluating the distance measurements at different design conditions. The accuracy distribution of the measurements indicated perfect agreement with the proposed diagram, which is then discussed in the last section of the paper.

2. Theoretical Background

Basic passive FMCW ranging systems measure the propagation time by mixing their transmit and receive sinusoidal chirp signals whose frequency linearly sweeps in time T_{fm} along a frequency bandwidth of B_{fm}. Mathematically, the transmit signal is modeled at a given time t as follows [6]:

$$s_{tx} = \text{rect}\left(\frac{t}{T_{fm}}\right) A\cos\left(2\pi f_o t + 2\pi\frac{\mu}{2}t^2\right), \tag{1}$$

where

$$\text{rect}\left(\frac{t}{T_{fm}}\right) = \begin{cases} 1 & 0 \le t \le T_{fm} \\ 0 & \text{others} \end{cases}, \tag{2}$$

where A is the signal amplitude, f_o is the frequency of the carrier signal, $\mu = \frac{B_{fm}}{T_{fm}}$ is the chirp modulation signal gradient. The frequency-modulated signal is transmitted, propagates at the speed-of-light c, then after a propagation delay $\tau/2$, it hits the target, bounces back, is received after the same propagation delay $\tau/2$, and τ represents the round-trip delay (RTD) time measurement to a passive reflector. Hence, $\text{rect}(t/T_{fm})$ limits the frequency-modulated signal to a time interval of T_{fm}. Similarly, the received reflected signal is a delayed version of the transmitted one that is mathematically expressed as follows:

$$s_{rx} = \text{rect}\left(\frac{t}{T_{fm}}\right) A\cos\left(2\pi f_o(t-\tau) + 2\pi\frac{\mu}{2}(t-\tau)^2\right). \tag{3}$$

The received signal is then mixed by a locally generated copy of the transmitted one and processed by a low-pass filter to produce a baseband beat signal $s_b(t)$, which is mathematically expressed as follows [1]:

$$s_b(t) = \text{rect}\left(\frac{t}{T_{fm}}\right)\frac{A}{2}\cos(\pi(2\mu\tau t + \mu\tau^2 + 2f_o\tau)). \tag{4}$$

Thus, the frequency of the beat signal can be calculated analytically by differentiating the instantaneous phase of the above beat signal with respect to time as follows:

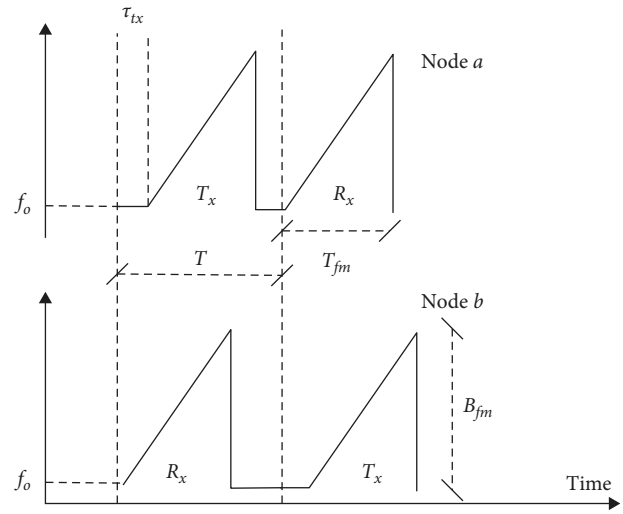

FIGURE 1: TWR FMCW timing diagram.

$$f_b = \frac{1}{2\pi}\frac{d}{dt}\pi(2\mu\tau t + \mu\tau^2 + 2f_o\tau) = \mu\tau. \tag{5}$$

Hence, the RTD, i.e., τ, is directly proportional to the frequency of the beat signal in the basic classical FMCW system. However, for the case of distance measurement between active transceiver nodes, each node mixes its chirp signal with a received signal from a remote one. Subsequently, the time delay between the mixed chirp signals does not only reflect the propagation time of the radio frequency (RF) signal but also includes a random time shift between a received and a locally generated reference chirp signal that represents the clock misalignment between the two transceiver nodes together with the propagation time.

3. Active TWR Measurement Protocol

Consider a system setup consisting of two transceiver nodes, each has an antenna switch that allows its RF front end to operate in either transmit or receive mode. In order to extract the distance measurement between the nodes, a TWR protocol is typically carried out by exchanging reference time measurement signals in both propagation directions. Thus, the measurement error caused by the clock misalignment is mathematically eliminated [2, 7]. As illustrated in Figure 1, one way to realize it is by dedicating a transmission time slot for each node. Consequently, one node listens to the transmitted signal from the other node and mixes it with its locally generated reference chirp signal. An extra time delay τ_{tx} is introduced to the transmission time frame T to guarantee a lagging transmit chirp signal mixing, where $\tau_{tx} \ll T_{fm}$. Briefly, as detailed in [2], a basic TWR measurement for a pair of nodes, a and b, involves the following steps:

(1) Node a transmits a reference signal that gets received by node b after a propagation time of τ.
(2) Node b mixes the received signal with its locally generated one, resulting in a beat signal whose frequency

value corresponds to a time difference of δ_b between the received and the locally generated reference chirp signal.

(3) After a time slot of T, node b transmits back its chirp signal, which is then received by node a and mixed with a locally generated signal. The resultant second beat signal has a frequency value that corresponds to a time difference of δ_a.

(4) The propagation time delay τ is calculated by summing up the two-time delay measurements, dividing by two, and finally subtracting τ_{tx} as follows:

$$\tau = (\delta_a + \delta_b)/2 - \tau_{tx}. \tag{6}$$

Thus, the measurement error due to the clocks' misalignment is canceled out by carrying out an FMCW time measurement in each transceiver node, as detailed in steps (1)–(3). Thereafter, the resultant time measurement is applied, as described in step (4), to extract the propagation time measurement between the two nodes. In practice, the RF signal propagates not only over a single line but also across multiple paths, producing a complex beat signal that contains multiple frequency components corresponding to the delay profile of the propagation paths.

4. Critical Design Considerations

Fundamentally, the above calculations of the time delay measures are applied after estimating the frequencies of the individual beat signals, which represent the raw output of the FMCW time measurement [7]. Such a frequency estimation is conventionally handled in the digital domain. Hence, it starts by properly sampling the resultant analog beat signal. Based on the Nyquist sampling theorem [8], a minimum valid sampling rate is double the maximum expected frequency of the beat signal that is, in turn, directly proportional to the time shift between the received and local chirp signals. Assuming a maximum time shift between the two transceiver nodes of τ_ε, a valid sampling rate of the beat signal must meet the following inequality:

$$f_s \geq 2\mu\tau_\varepsilon, \tag{7}$$

which represents a minimum valid sampling frequency for a given chirp gradient μ. Furthermore, as the accuracy of the frequency estimation is limited by the spectral bin resolution, deciding for a proper sampling rate is, in fact, dictated by the signal bandwidth [9], too, and can be expressed for the case of TWR system as follows:

$$\tau_\Delta \geq \frac{1}{B_{fm}}, \tag{8}$$

where τ_Δ is the time resolution of the underlying measurement. In turn, it can be represented according to Equation (5) by its equivalent beat signal frequency resolution f_Δ as follows:

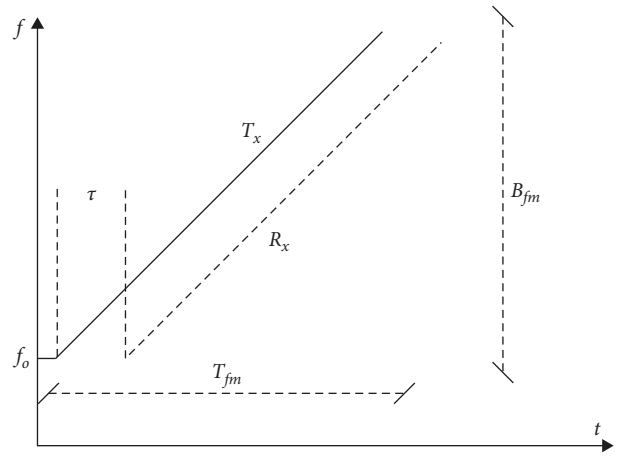

FIGURE 2: FMCW chirp signal.

$$f_\Delta \leq \frac{\mu}{B_{fm}}. \tag{9}$$

Mathematically, the sampling rate can be described as a multiple of the spectral resolution by the total number of samples N, i.e., $f_s = f_\Delta N$. Thus, Equation (9) extends to the following inequality:

$$f_s \leq \frac{\mu N}{B_{fm}}. \tag{10}$$

Combining Equations (7) and (10), altogether, a valid sampling rate should satisfy the following inequality:

$$2\mu\tau_\varepsilon \leq f_s \leq \frac{\mu N}{B_{fm}}. \tag{11}$$

Foremost, simplifying the above inequality where only the left and right sides are considered, an indication on the maximum valid bandwidth of the ranging system is calculated as follows:

$$B_{fm} \leq \frac{N}{2\tau_\varepsilon}. \tag{12}$$

Thereafter, breaking out the inequality (11) in terms of the chirp duration, considering $\mu = \frac{B_{fm}}{T_{fm}}$, as shown in Figure 2, results in the following two conditions on the valid sampling frequency. The first one is referred to as the spectral length condition,

$$f_s^a\left(T_{fm}\right) \leq \frac{N}{T_{fm}}, \tag{13}$$

and the second one is referred to as the bandwidth/time ambiguity condition,

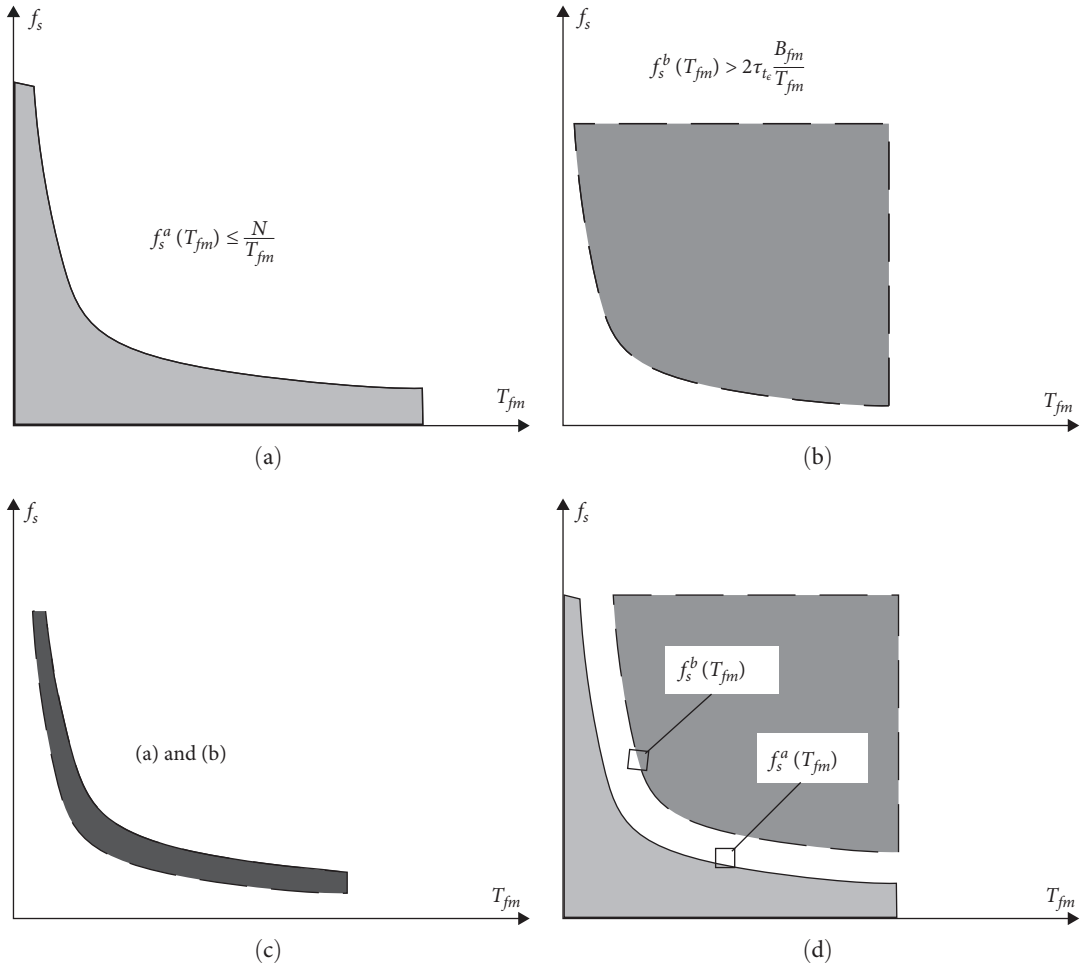

FIGURE 3: Illustration diagram at (a) condition of Equation (13), (b) condition of Equation (14), (c) valid operation intersection area, and (d) invalid conditions.

$$f_s^b\left(T_{fm}\right) \ge 2\tau_\varepsilon \frac{B_{fm}}{T_{fm}}. \tag{14}$$

The first condition defines a maximum sampling rate under a given spectral length N as a function of chirp duration T_{fm}, and the second condition defines a minimum sampling rate under a given frequency bandwidth and synchronization time ambiguity as a function of chirp duration T_{fm}. As illustrated in Figure 3, an intersection area between the two functions represents a subset of (f_s, T_{fm}) pairs which defines a valid two-way ranging diagram (VTRD). Remarkably, examining the VTRD, one can directly visualize how critical is the ranging system design under the given constraints of B_{fm}, τ_ε, and N. Particularly, a larger intersection area indicates relaxed conditions on deciding the sampling rate and chirp length and vice versa. Furthermore, one can easily determine the existence of the intersection area and decide whether there is a valid condition at all. Yet, in practical FMCW TWR systems, interpolation might be carried out to achieve higher accuracy on the spectral peak estimation. In this case, zero-padding is typically applied to the sampled beat signal to deliver higher spectral bin resolution [10]. Thus, following the above calculations under the assumption of zero padding, the inequality (10) extends to the following:

$$2\mu\tau_\varepsilon \le f_s \le \frac{\mu\eta N}{B_{fm}}, \tag{15}$$

where η represents the percentage of the beat signal samples occupied to the total zero-padded samples. It is worth mentioning that special attention should be paid to the above mathematical calculations when using a different timing protocol than the one shown in Figure 1.

The above boundaries are essential design considerations for a valid TWR system. In contrast, for the ultimate possible accuracy calculation, the Cramér–Rao bound is typically applied to provide the best theoretical distance precision under a given signal-to-noise ratio (SNR) and total number of samples [11]. Furthermore, apart from the mentioned parameters, deeper considerations such as SNR, phase noise, and Doppler shift are detailed in the literature and should accordingly be

Table 1: Simulated active ranging design constraints.

Parameter	Scenario				Unit
	A	B	C	D	—
B_{fm}	10	50	150	150	MHz
τ_ε	10	10	1	20	μs
N	1,024	1,024	1,024	8,192	Sample

integrated into the above boundaries for more accurate qualification of a TWR system [12].

5. Monte-Carlo Simulation

This section briefly discusses a Monte-Carlo model of a TWR system that simulates the expected measurement performance under arbitrary design conditions. Hence, the accuracy of the distance measurements can statistically be evaluated for a large number of system design parameters. Ideally, modeling an FMCW TWR system requires generating its modulated RF signals, as illustrated in Figure 2. However, such a model demands a relatively high sampling rate, which results in a complex simulation environment. Instead, a simplified model of the beat baseband signal is considered, which relaxes the mathematical calculations and resembles enough information to simulate the expected distance measurement accuracy. Thus, the beat signal is represented in Equation (4) by modeling a sinusoidal signal whose frequency is directly proportional to a modeled time difference of the reference FMCW RF signals. Furthermore, an arbitrary multipath tone signal that resembles a maximum propagation path length of about twice the expected spacial resolution is included by superimposing an extra sinusoidal component to the ideal beat signal at a corresponding beat frequency value. Assuming a given design specifications of B_{fm}, τ_ε, and N, each simulation point represents a TWR system operating at an arbitrary T_{fm} and f_s. The frequencies of the resultant beat signals are estimated by a fast Fourier transform (FFT) process followed by a spectral peak detection with parabolic interpolation. In order to limit the simulation window, a minimum and maximum T_{fm} are set to 25 μs and 2.5 ms, accordingly.

Four design scenarios, as listed in Table 1, are simulated. Thereafter, for each simulation point, the FMCW TWR ranging process is carried out according to Equation (6) for 10 runs, and the one with the poorest accuracy is chosen to represent the worst-case accuracy at that simulation point. As shown in Figures 4(a), 4(c), and 4(d), the simulation model resulted in a clear, distinct border around a set of high-accuracy simulation points, which coincides with the two condition curves of the proposed VTRD (Equations (13) and (14)). Yet, the resultant ranging accuracy of scenario (B), as shown in Figure 4(b), was extremely bad with no clear VTRD. Here, the condition curves of the VTRD are not satisfied, thus no intersection area is expected. In practice, in order to maintain the desired frequency bandwidth and bring the system to a working condition, one can either enhance the time ambiguity τ_ε or increase the number of the processing samples N. As a result, one can remark a distinct contrast in the system performance with a dramatic degradation in the measurement accuracy when the VTRD design conditions curves are disregarded.

6. Laboratory Test

Similar to the simulation model, the test of the proposed VTRD diagram in a practical FMCW setup necessitates a system with a variable sampling rate and configurable chirp settings, thus evaluating the quality of the resultant measurements accordingly. However, practical systems are frequently constrained by restricted signal design configurations and generally sample the baseband signal at a specified sampling rate for their optimal performance. Nonetheless, in order to generate a configurable chirp signal, a laboratory setup is assembled to carry out the required test measurements. As illustrated in Figures 5 and 6, the setup consists of a signal generator (R&S: SMA100B) [13], a real-time oscilloscope with a bandwidth of 4 GHz (R&S: RTO-2044) [14], and a low-noise amplifier (LNA) (ZVE-8G) [15] whose gain is around 30 dB and noise figure is about 4 dB. The signal generator provides good flexibility in generating the required chirp signal in terms of its duration, staring frequency, and gradient. Furthermore, sampling the RF signal at an appropriate rate with a real-time oscilloscope enables postprocessing of the baseband signal to emulate different sampling rates. The design constraints of the experimental setup are listed in Table 2. In detail, the FMCW signal is generated at around 2.42 GHz and a bandwidth, limited by the signal generator, of around 40 MHz. Thereafter, the generated RF signal is split through a power divider. One output path is connected to a rod antenna while the other path is fed to a 2 m long coaxial cable that provides an ideal reference FMCW signal. Although the coaxial cable has typically a lower velocity factor than the wireless link [16], the delays of the two paths are expected to be identical as the total group delay of the mixer and antennas setup happen to balance the delay difference between the cable and the wireless propagation paths. At the receiver side, the propagated RF signal is captured by another rod antenna connected through the LNA along with the reference cable signal and fed into two individual channels of the oscilloscope running at a sampling rate of about 10 GSample/s. Such a rate is essential to ensure proper sampling of the RF signal for the postprocessing calculations. However, due to the high sampling rate, a major limitation of the measurement setup is the maximum signal duration of the oscilloscope's capture window length of around 1 ms. Thus, four equally spaced chirp duration times are selected along that 1 ms window, and a variable sampling rate of the beat signal is emulated in post-processing, as shown in Figure 5, in which L denotes a decimation factor of a downsampling operation to an arbitrary signal sampling rate. A multipath propagation is modeled by superimposing a copy of the sampled cable signal with a variable delay value. Finally, the frequencies of the resultant beat signals are estimated by an FFT process followed by a spectral peak detection with parabolic interpolation. Hence, a close procedure to the simulation model is applied. As a result, then the accuracy of the distance

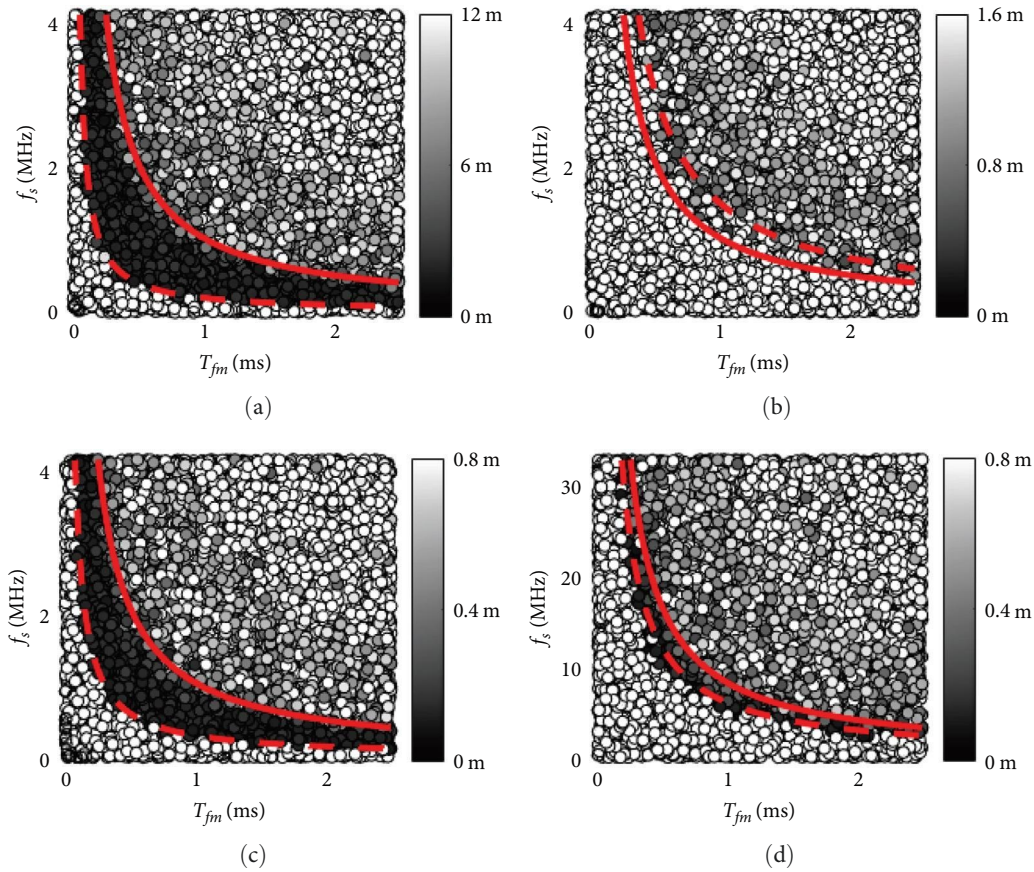

FIGURE 4: Monte-Carlo simulation ranging accuracy outcomes indicated in a grayscale of (a) scenario A, (b) scenario B, (c) scenario C, and (d) scenario D. Solid line is condition of Equation (13), dashed line is condition of Equation (14), and the circles are the simulation points. For the sake of visualization, the plotted accuracy values are truncated to the expected special-ranging resolution of the given bandwidth.

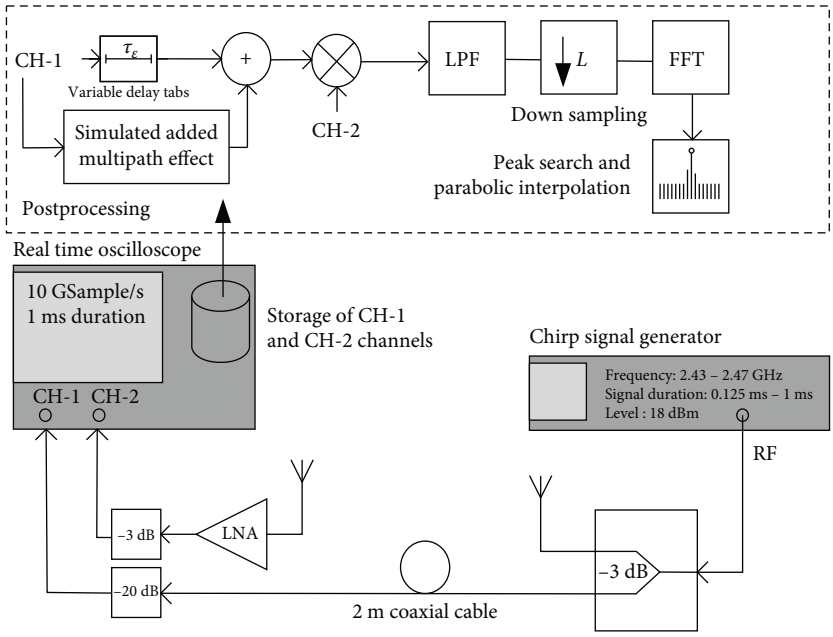

FIGURE 5: A block diagram of the experimental setup.

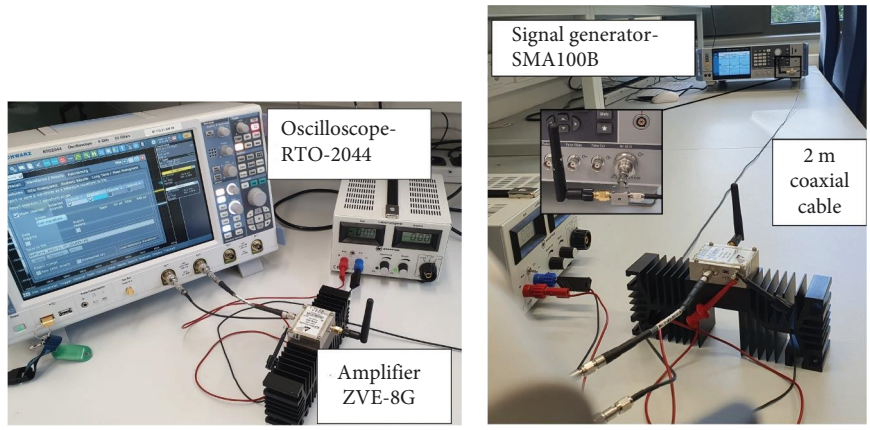

(a) (b)

Figure 6: Experimental laboratory setup: (a) oscilloscope/LNA receiver; (b) chirp signal generator view.

Table 2: Experimental setup constraints.

Parameter	Value	Unit
B_{fm}	40	MHz
τ_ε	5	μs
N	1,024	Samples
Maximum T_{fm}	1	ms

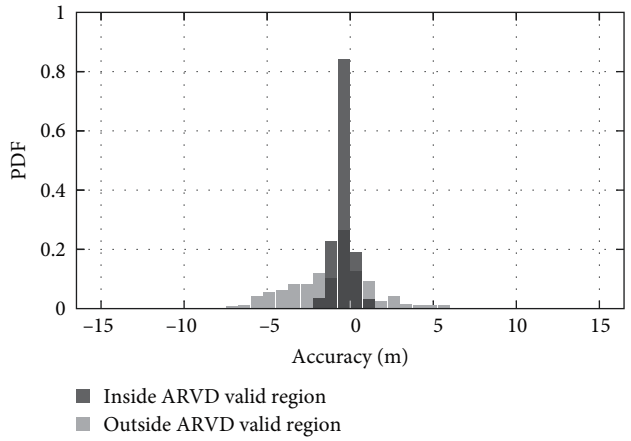

Figure 7: Measurement's accuracy PDF. Outliers measurements due to the unrealistic f_s and T_{fm} selection are excluded from the plot for enhanced visualization.

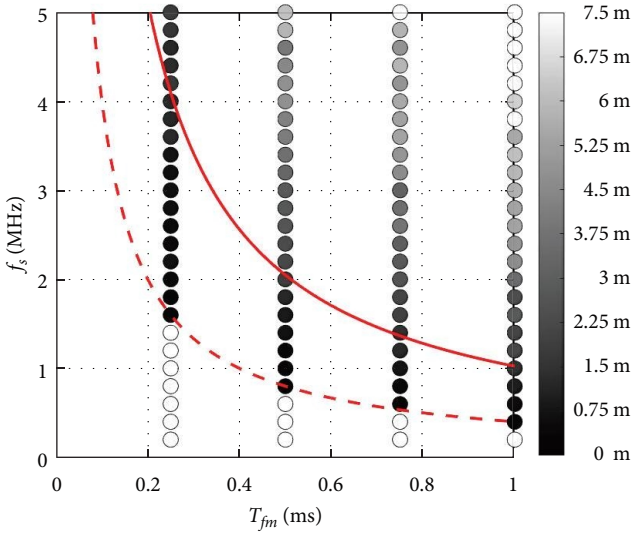

Figure 8: Experimental ranging absolute accuracy distribution.

measurements is calculated. This, as in the simulation, shows a clear, high-accuracy region between the two conditions curved; thus, it has a very good agreement with the expected VTRD. In order to shed more light on the distinct valid borders, the measurement points are categorized according to their position on the VTRD into two sets, one of which is for the points inside the valid area, and the other is for the rest of the measurement points. As shown in Figure 7, the probability density function (PDF) curve of the valid region measurements implies a clear sharpness when compared to the PDF curve of the other set. Additionally, several points are excluded from the invalid set of measurements due to their extreme inaccuracy as a result of the invalid operation conditions.

7. Discussion and Conclusion

A valid operation design diagram was proposed for the case of an FMCW time-based TWR synchronization protocol. The proposed diagram represents an intersection area of two boundary curves that indicate the functionality of the system at a given frequency bandwidth, spectral length, and clock synchronization ambiguity. Examining the outcomes of the simulation model, the first scenario (A) has a relatively high τ_ε of 10 μs, which models a typical TWR issue of a poor time synchronization condition. Nevertheless, according to the calculated maximum bandwidth as in Equation (12), it has relaxed working conditions. Thus, the VTRD and its calculated accuracy distribution both indicated a clear valid operation region. The second scenario (B), in contrast, features a wider frequency bandwidth, which in turn pushes

the measurement model into an invalid working condition. Hence, its VTRD did not indicate a possible valid operation area at all. In this particular case, the dashed boundary curve of condition (14) lies above the solid one of condition (13). The third design scenario had an even higher bandwidth than scenario (B), yet its maximum τ_ε is 10 times enhanced, which resulted in a clear VTRD area. Finally, the fourth design scenario (D) models a system that features a bandwidth equal to scenario (C) and an even worse clock synchronization, yet it has eight times longer spectral length. As a result, it has a thin VTRD operation area that indicates the existence of valid conditions.

Proceeding to the practical laboratory setup, as shown in Figures 7 and 8, the measurement points inside the VTRD region resulted in a clear gathering of high-accuracy measurements. Furthermore, examining the PDF curves, the set of measurements inside the VTRD region has a sharper PDF distribution than the rest, which implies their high distance measurement accuracy in comparison to the rest of the measurements.

In conclusion, the proposed VTRD provides an intuitive illustration about the valid design conditions of the TWR FMCW system that helps to optimize the design parameters prior to the complexity of system development.

Data Availability

The data used to support the findings of this study are available from the corresponding author upon reasonable request.

Conflicts of Interest

The authors declare that they have no conflicts of interest.

Acknowledgments

This research was partially funded by the EU's Framework Program H2020 under grant agreement number 876487 (NextPerception) and by the Deutsche Forschungsgemeinschaft (DFG, German Research Foundation) via a Major Instrumentation Initiative with identification number 434434888. Moreover, we would like to acknowledge the cooperation with the DFG Cluster of Excellence CeTI, the DFG research hub 6G-life, and the Zukunftscluster SEMECO supported by the BMBF (Federal Ministry of Education and Research). Open Access funding enabled and organized by Projekt DEAL.

References

[1] Y. S. Cho and S. H. Cho, "A design of the frequency modulated continuous wave (FMCW) radar system," in *The 18th IEEE International Symposium on Consumer Electronics (ISCE 2014)*, pp. 1-2, IEEE, Jeju, Korea (South), 2014.

[2] B. Al-Qudsi, N. Joram, M. El-Shennawy, and F. Ellinger, "Scalable indoor positioning system with multi-band FMCW," *IET Radar, Sonar & Navigation*, vol. 12, no. 1, pp. 46–55, 2018.

[3] L. Zamora-Cadenas, N. Arrue, A. Jiménez-Irastorza, and I. Vélez, "Improving the performance of an FMCW indoor localization system by optimizing the ranging estimator," in *2010 6th International Conference on Wireless and Mobile Communications*, pp. 226–231, ACM, 2010.

[4] I. Domuta and T. P. Palade, "Two-way ranging algorithms for clock error compensation," *IEEE Transactions on Vehicular Technology*, vol. 70, no. 8, pp. 8237–8250, 2021.

[5] R. Y. C. L. Dias and T. Liu, "Designing, measurement and analysis of a short range fmcw radar," in *2019 4th International Conference on Electromechanical Control Technology and Transportation (ICECTT)*, pp. 138–141, IEEE, Guilin, China, 2019.

[6] Y. Li and S. O'Young, "Focusing bistatic FMCW SAR signal by range migration algorithm based on fresnel approximation," *Sensors*, vol. 15, no. 12, pp. 32123–32137, 2015.

[7] B. Al-Qudsi, M. El-Shennawy, N. Joram, and F. Ellinger, "Crystal oscillator frequency offset compensation for accurate FMCW radar ranging," in *2016 German Microwave Conference (GeMiC)*, pp. 405–408, IEEE, 2016.

[8] H. Nyquist, "Certain factors affecting telegraph speed," *Bell System Technical Journal*, vol. 3, no. 2, pp. 324–346, 1924.

[9] H.-H. Ko, K.-W. Cheng, and H.-J. Su, "Range resolution improvement for FMCW radars," in *2008 European Radar Conference*, pp. 352–355, IEEE, Amsterdam, Netherlands, 2008.

[10] A. Al Teneiji, M. S. Khan, N. Ali, and A. Al Tunaiji, "Improving the detection accuracy of frequency modulated continuous wave radar," in *2018 International Conference on Signal Processing and Information Security (ICSPIS)*, pp. 1–4, IEEE, DUBAI, United Arab Emirates, 2018.

[11] S. Scherr, S. Ayhan, M. Pauli, and T. Zwick, "Accuracy limits of a K-band FMCW radar with phase evaluation," in *2012 9th European Radar Conference*, pp. 246–249, IEEE, Amsterdam, Netherlands, 2012.

[12] M. El-Shennawy, B. Al-Qudsi, N. Joram, and F. Ellinger, "Fundamental limitations of phase noise on FMCW radar precision," in *2016 IEEE International Conference on Electronics, Circuits and Systems (ICECS)*, pp. 444–447, Monte Carlo, Monaco, 2016.

[13] Rohde and Schwarz, "R&S SMA100B RF and microwave signal generator specifications," Datasheet version 07.01, 2022.

[14] Rohde and Schwarz, "R&S RTO oscilloscope specifications," Datasheet version 30.01, 2021.

[15] Mini-Circuits, "Coaxial amplifier ZVE-8G+, ZVE-8G," Rev. A M113418 ZVE-8G

[16] B. H. Saoudi, "Analysis and study the performance of coaxial cable passed on different dielectrics," *International Journal of Applied Engineering Research*, vol. 13, no. 3, pp. 1664–1669, 2018.